

Research Article

Molecular Docking Investigation, Pharmacokinetic Analysis, and Molecular Dynamic Simulation of Some Benzoxaborole-Benzimidazole Hybrids: An Approach to Identifying Superior *Onchocerca* Inhibitors

Fabian Audu Ugbe* 

Gideon Adamu Shallangwa 

Adamu Uzairu 

Ibrahim Abdulkadir 

Department of Chemistry, Ahmadu Bello University, Zaria, Kaduna State, Nigeria

*email: ugbefabianaudu@gmail.com

Keywords:

Benzimidazole-benzoxaborole
Flubendazole
Molecular docking
Molecular dynamics
Onchocerciasis
Pharmacokinetics

Abstract

Onchocerciasis is one of the major neglected tropical diseases caused by the filarial worm (*Onchocerca volvulus*), affecting an estimated population of about 37 million people living predominantly in tropical Africa. The major treatment approach has been based on the use of Ivermectin, which kills the microfilariae or the less effective Doxycycline targeting *Wolbachia*, endosymbiont of filarial nematodes. Flubendazole (FBZ) has proved effective in treating adult worms but with threatening adverse effects. Against this backdrop, therefore, a combined molecular docking study and pharmacokinetic screening were conducted on a series of benzimidazole-benzoxaborole hybrids to find more potent analogs with attributes that address the limitations of existing therapies. All the nineteen analogs were found to possess better docking scores than the reference drug (FBZ, Moldock scores = -120.466 and -125.359). The results of pharmacokinetic testing suggest that four molecules (**14**, **16**, **19**, and **20**) are orally bioavailable and showed better ADMET properties than FBZ. These molecules and FBZ showed good binding interactions with the receptors' active sites. Also, the molecular dynamic simulation performed on the docked complexes of **20** and FBZ confirmed the rigidity and stability of their interactions. Based on the results of this study, the selected molecules (especially **20**) could be considered superior drug candidates for the treatment of Onchocerciasis.

Received: August 20th, 2022

1st Revised: January 30th, 2023

Accepted: February 20th, 2023

Published: February 28th, 2023



© 2023 Fabian Audu Ugbe, Gideon Adamu Shallangwa, Adamu Uzairu, Ibrahim Abdulkadir. Published by Institute for Research and Community Services Universitas Muhammadiyah Palangkaraya. This is an Open Access article under the CC-BY-SA License (<http://creativecommons.org/licenses/by-sa/4.0/>). DOI: <https://doi.org/10.33084/bjop.v6i1.3876>

INTRODUCTION

Onchocerciasis, otherwise known as river blindness, is identified as one of the neglected tropical diseases by the World Health Assembly resolutions, which has raised a major public health concern¹. It is a vector-borne filarial infection majorly caused by *Onchocerca volvulus*, a filarial nematode transmitted from human to human through the bite of the female blackflies². This infection is more prevalent in tropical Africa, where according to the World Health Organization, an estimated population of about 37 million people has the infection, and a further 300,000 people are blind from the infection³. Onchocerciasis is associated with such conditions as skin rashes, disfiguring skin changes, blindness, musculoskeletal issues, weight loss, and immune system disorders⁴. Furthermore, onchocerciasis brings about long-term disability, poor productivity by the affected populace, social stigmatization, and poor economic growth, among others⁵.

Ivermectin (IVM) is the latest recommended treatment for onchocerciasis but is not to be used in co-endemic areas for loiasis owing to potentially serious adverse effects⁶. Over the years, microfilariae have been the target of treatment with IVM, the most widely administered drug for treating onchocerciasis due to its good tolerance level and high efficacy¹. A prolonged

How to cite: Ugbe FA, Shallangwa GA, Uzairu A, Abdulkadir I. Molecular Docking Investigation, Pharmacokinetic Analysis, and Molecular Dynamic Simulation of Some Benzoxaborole-Benzimidazole Hybrids: An Approach to Identifying Superior *Onchocerca* Inhibitors. Borneo J Pharm. 2023;6(1):58-78. doi:10.33084/bjop.v6i1.3876

yearly IVM therapy of not less than 10 to 15 years was predicted to be required to eliminate onchocerciasis in humans. More so, a research report in Central Africa during the treatment of onchocerciasis with IVM suggests that several adverse effects were recorded, such as encephalopathy and death for patients already infected with *Loa loa*³. Another treatment approach is doxycycline, an antibiotic targeting the bacteria organism *Wolbachia* which co-habits with filarial nematodes in a somewhat endosymbiotic fashion. Doxycycline is, however, not compelling enough for mass drug administration due to its long treatment period of 4-6 weeks and contraindication in children and pregnancy².

A useful class of compounds with a broad spectrum of anti-helminthic activity is the benzimidazoles which kill both larvae and adult nematodes with generally low human toxicity except that they are associated with teratogenicity and embryotoxicity⁷. Principal members of this class include mebendazole, flubendazole (FBZ), and albendazole⁸. FBZ is an approved drug for treating gastrointestinal nematodes in humans. It has also been reported as an active agent against organisms causing onchocerciasis and with close to 100% efficacy against macrofilariae when given parenterally because it is poorly absorbed⁸. This is, however, associated with local tissue reactions at the injection site. Also, no report has certified FBZ safe in pregnancy and animal studies.

As a result of the great promise shown by FBZ, some institutions formed a partnership in 2011 to develop FBZ in suitable oral formulation alongside other relevant pharmacological studies⁸. It was earlier reported that benzoxaborole core can significantly improve the solubility and hence the oral bioavailability of poorly soluble molecules⁹. The continuous search for a more potent anti-onchocerca agent that overcomes the side effects of existing therapies motivated Akama *et al.*⁹ and Carter *et al.*¹⁰ to synthesize a series of benzoxaborole-benzimidazole analogs of FBZ that would eliminate the limitations. Consequently, this study is focused on the computer-aided modeling of the benzoxaborole-benzimidazole hybrids as novel *Onchocerca* inhibitors while comparing the same with FBZ, a promising benzimidazole compound.

Computer-aided drug design is crucial in discovering new drug molecules in pharmaceutical design, drug metabolism, and medicinal chemistry. It saves time and cost and tends to be highly effective for evaluating a sizeable virtual database of chemical compounds¹¹. Molecular docking simulation is a computer-aided screening method that probes the binding of ligands in the active sites of the protein target using a valid docking tool¹². Pharmacokinetics analysis, on the other hand, is essential in the pre-clinical study of new drug compounds to ascertain how much drug compounds affect the living organism when administered. Some of the most important pharmacokinetic properties to be determined during pre-clinical testing include Absorption, Distribution, Metabolism, Excretion, and Toxicity (ADMET)^{13,14}. Physico-chemical properties such as molecular weight, Topological Polar Surface Area (TPSA), lipophilicity indices, Hydrogen Bond Donors (HBD), and Hydrogen Bond Acceptors (HBA), amongst others, are necessary to predict a drug's likelihood of being orally bioavailable¹⁵. Molecular Dynamic (MD) simulation tends to probe the stability of the protein-ligand interactions in a dynamically perturbed system¹⁶.

Two interesting therapeutic protein targets of *O. volvulus* were used for this study: prostaglandin D synthase (PDB: 2HNL) and pi-class glutathione S-transferase (PDB: 1TU7), both of which are of the enzyme class transferase and function similarly. *Onchocerca volvulus* can survive in any competent host with a well-built immune system because it employs a variety of defense mechanisms, not excluding the mechanisms of detoxification and repair of the glutathione S-transferases¹⁷. These enzymes, therefore, have the ability to partake in the immune response modulation to prevent the damaging effect of their host's effector responses, thereby making them suitable drug targets for the development of new therapies and vaccines¹⁸. In this study, a virtual molecular docking screening, prediction of pharmacokinetic properties, and MD simulation were conducted on some benzoxaborole-benzimidazole hybrids to find a more suitable drug candidate that would be used for the treatment of onchocerciasis.

MATERIALS AND METHODS

Materials

The hardware used was an HP laptop computer with the following specifications: Processor (Intel® Core™ i5-4210U CPU @ 1.70 GHz 2.40 GHz), Installed RAM (8.00 GB), System Type (64-bit operating system, x64-based processor), Edition (Windows 10 Home Single Language), Version 21H2. Software used includes Chemdraw Ultra v. 12.0.2, Spartan '14 v. 1.1.4, and Biovia Discovery Studio Visualizer v.16.1.0.15350. Others include Molegro Virtual Docker v. 6.0, a product of the A CLC

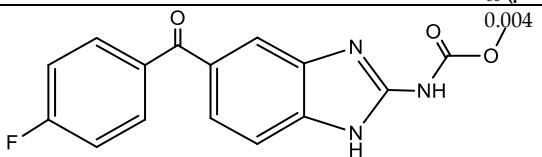
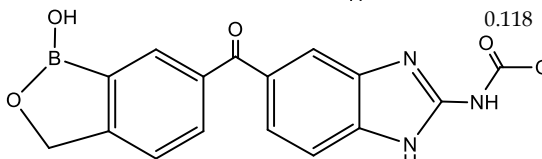
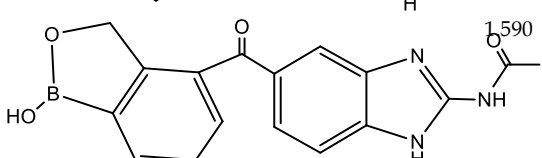
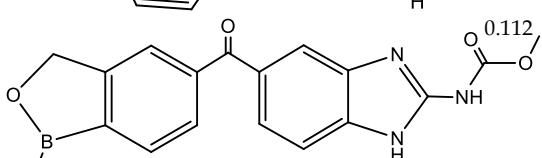
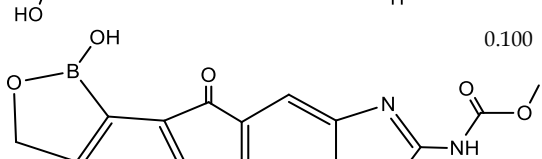
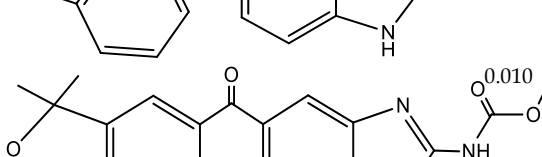
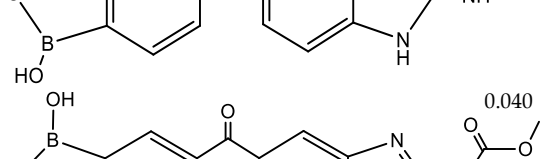
Bio Company, NAMD v.2.14, and VMD v.1.9.3 OpenGL Display. The online web servers: SwissADME (<http://www.swissadme.ch/index.php>); pkCSM (<http://biosig.unimelb.edu.au/pkcsm>); admetSAR (<http://lmm.d.ecust.edu.cn/admetSar2>); and PAINS-Remover (<https://www.cbligand.org/PAINS/>) were used for the pharmacokinetics properties prediction; while CHARMM-GUI (<https://www.charmm-gui.org>) was used for generating ligand parameter files for MD simulation¹⁹⁻²³.

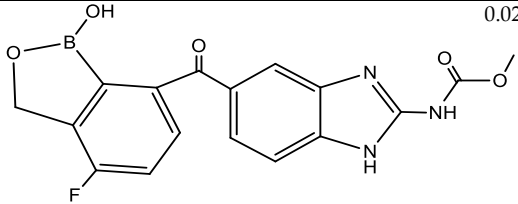
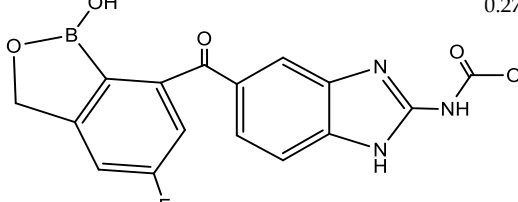
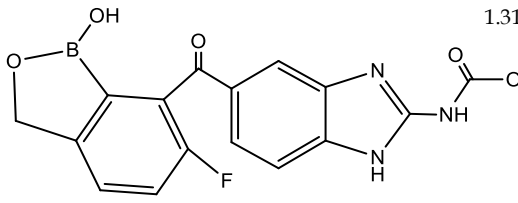
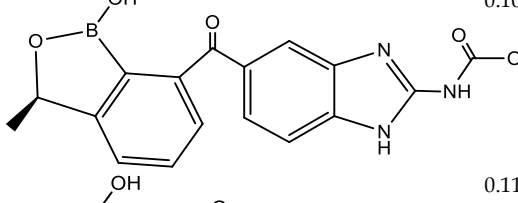
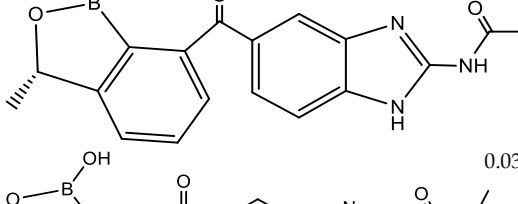
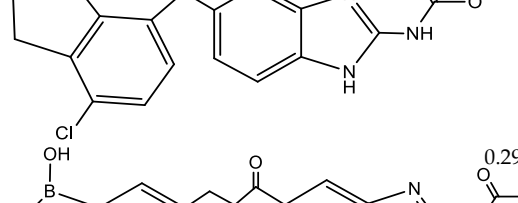
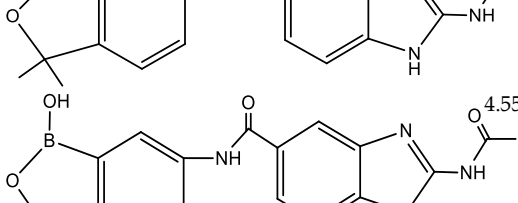
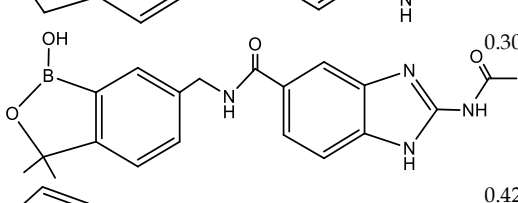
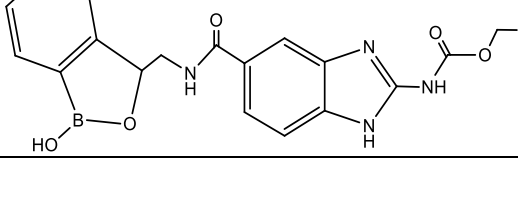
Methods

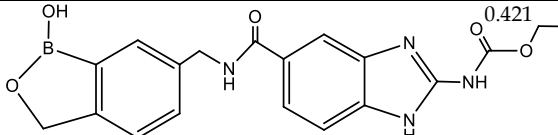
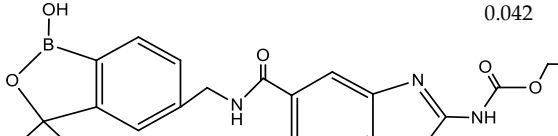
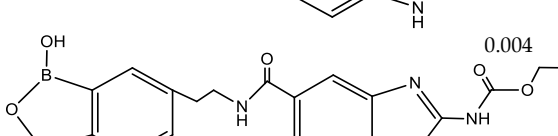
Data sourcing

Akama *et al.*⁹ and Carter *et al.*¹⁰ reported the synthesis of a series of amide-linked and ketone-linked analogs of benzoxaborole-benzimidazole hybrid, respectively, as well as FBZ, as part of the anti-Onchocerca drug discovery effort. Their biological activities were tested against *O. volvulus* L3 larval molting assay and reported in micromolar (μM). Consequently, a dataset of 20 compounds comprising FBZ and benzoxaborole-benzimidazole analogs with relatively better half-maximal inhibitory concentration (IC_{50}) values was obtained from their report and used for this theoretical study. The molecular structures, bioactivities (IC_{50}), and pIC_{50} obtained as a logarithmic function of IC_{50} for these compounds were reported in **Table I**.

Table I. Molecular structures, observed activities, and SMILES strings of FBZ and the various benzimidazole-benzoxaborole hybrids

ID	Molecular structures	IC_{50} (μM)	pIC_{50}	SMILES
1*		0.004	8.3979	<chem>COC(=O)NC1=NC2=CC(=CC=C2N1)C(=O)C1=CC=C(F)C=C1</chem>
2		0.118	6.9281	<chem>COC(=O)NC1=NC2=CC(=CC=C2N1)C(=O)C1=CC2=C(COB2O)C=C1</chem>
3		1.590	5.7986	<chem>COC(=O)NC1=NC2=CC(=CC=C2N1)C(=O)C1=CC=CC2=C1COB2O</chem>
4		0.112	6.9508	<chem>COC(=O)NC1=NC2=CC(=CC=C2N1)C(=O)C1=CC2=C(C=C1)B(O)OC2</chem>
5		0.100	7.0000	<chem>COC(=O)NC1=NC2=CC(=CC=C2N1)C(=O)C1=CC=CC2=C1B(O)OC2</chem>
6		0.010	8.0000	<chem>COC(=O)NC1=NC2=CC(=CC=C2N1)C(=O)C1=CC2=C(C=C1)B(O)OC2(C)C</chem>
7		0.040	7.3979	<chem>COC(=O)NC1=NC2=CC(=CC=C2N1)C(=O)C1=CC2=C(C=C1)[C@H](C)OB2O</chem>

8		0.020	7.6990	<chem>COC(=O)NC1=NC2=CC(=CC=C2N1)C(=O)C1=CC=C(F)C2=C1B(O)OC2</chem>
9		0.270	6.5686	<chem>COC(=O)NC1=NC2=CC(=CC=C2N1)C(=O)C1=CC(F)=CC2=C1B(O)OC2</chem>
10		1.310	5.8827	<chem>COC(=O)NC1=NC2=CC(=CC=C2N1)C(=O)C1=C(F)C=CC2=C1B(O)OC2</chem>
11		0.100	7.0000	<chem>COC(=O)NC1=NC2=CC(=CC=C2N1)C(=O)C1=CC=CC2=C1B(O)O[C@@H]2C</chem>
12		0.110	6.9586	<chem>COC(=O)NC1=NC2=CC(=CC=C2N1)C(=O)C1=CC=CC2=C1B(O)O[C@H]2C</chem>
13		0.030	7.5229	<chem>COC(=O)NC1=NC2=CC(=CC=C2N1)C(=O)C1=CC=C(Cl)C2=C1B(O)OC2</chem>
14		0.290	6.5376	<chem>COC(=O)NC1=NC2=CC(=CC=C2N1)C(=O)CCCC1=CC2=C(C=C1)C(C)(C)OB2O</chem>
15		4.550	5.3420	<chem>CCOC(=O)NC1=NC2=CC(=CC=C2N1)C(=O)NC1=CC2=C(COB2O)C=C1</chem>
16		0.300	6.5229	<chem>CCOC(=O)NC1=NC2=CC(=CC=C2N1)C(=O)NCC1=CC2=C(C=C1)C(C)(C)OB2O</chem>
17		0.426	6.3706	<chem>CCOC(=O)NC1=NC2=CC(=CC=C2N1)C(=O)NCC1OB(O)C2=C1C=CC=C2</chem>

18		0.421	6.3757	<chem>CCOC(=O)NC1=NC2=CC(=CC=C2N1)C(=O)NCC1=CC2=C(COB2O)C=C1</chem>
19		0.042	7.3768	<chem>CCOC(=O)NC1=NC2=CC(=CC=C2N1)C(=O)NCC1=CC2=C(C=C1)B(O)OC2(C)C</chem>
20		0.004	8.3979	<chem>CCOC(=O)NC1=NC2=CC(=CC=C2N1)C(=O)NCCC1=CC2=C(C=C1)C(C)(C)OB2O</chem>

Note: 1* - Flubendazole (FBZ)

Structural optimization

The molecular structures of all the compounds in **Table I** were drawn using the ChemDraw Ultra, saved as MDL molfile format and fed separately onto the Spartan '14 Graphical User Interface. Energy minimization was performed on the imported molecules and then saved in Spartan file format. The resulting structures were then subjected to full-scale optimization first by using Molecular Mechanics Force Field (MMFF) and after that, Density Functional Theory (DFT) with Becke's three-parameter read-Yang-Parr hybrid (B3LYP) option and utilizing the 6-31G** basis set. The optimized structures were saved as PDB formats for subsequent use in molecular docking studies^{13,24}.

Docking protocol

The crystal structures of two *O. volvulus* target proteins, prostaglandin D synthase (PDB: 2HNL) and pi-class glutathione S-transferase (PDB: 1TU7), were retrieved from the RCSB Protein Data Bank in the PDB file format and then modified separately using the Molegro Virtual Docker (MVD) by eliminating water molecules, cofactors, and co-crystallized ligands contained within the protein structures²⁵. Both proteins comprise similar chains (A and B), while A was utilized. The software allows for the repair (rebuild) of all affected residues. The receptor's binding cavities were defined, and those which have the largest volume and surface areas (volume: 38.912 and 33.28; surface: 139.52 and 144.64) for 2HNL and 1TU7 respectively, were adopted for the docking. All ligands were imported in PDB file format and prepared appropriately. The simulation was performed using the parameter settings in **Table II**. The binding scores were then recorded, while the predicted ligand-protein interaction profiles were visualized using the Biovia Discovery Studio Visualizer. A similar method was earlier reported elsewhere^{14,26}.

Prediction of pharmacokinetic properties

Drug-likeness and ADMET properties prediction constitute a vital stage in drug discovery's early phase because only molecules with good drug-likeness properties and excellent ADMET profiles advance into the pre-clinical research phase¹³. Here, FBZ and the selected compounds (**6**, **14**, **15**, **16**, **18**, **19**, and **20**) with the best binding scores were investigated for their pharmacokinetic properties using three online web servers: SwissADME, pkCSM, and admetSAR for drug-likeness, ADME and toxicity profiling respectively. The choices of molecules for oral bioavailability have been guided by several rules such as Lipinski's 'rule of 5' (RO5), Veber rule, Ghose rule, Egan, Muegge, and others²⁷. Lipinski's RO5 is a widely used criterion for oral bioavailability. As such, these compounds would be assessed for oral bioavailability using the RO5 criteria¹⁵.

Molecular dynamics simulation

Molecular dynamics (MD) simulations of the complexes of compound **20** with both proteins (2HNL and 1TU7) were performed separately using the combined approach of Chemistry at Harvard Macromolecular Mechanics (CHARMM) force field, Nano-scale Molecular Dynamics (NAMD), and Visual Molecular Dynamics (VMD). The CHARMM-GUI, an established web-based platform that utilizes the CHARMM force field, was used to generate the input files for the simulation by NAMD²³. The periodic boundary condition was utilized while fitting the system into a cubic water box for solvation. The protein was solvated and neutralized explicitly in an aqueous solution of 0.1 M KCl salt¹⁶. Energy minimization was performed to stabilize the complex structure and ensure steric clashes will not result. The resulting system

of ions and solvent was then equilibrated to stabilize the system at a temperature chosen for the simulation (310 K) at a constant number of particles, volume, and temperature (NVT ensemble) and to stabilize the pressure by keeping the number of particles, pressure, and temperature (NPT ensemble) constant using 100 ps time frame²⁸. MD was then performed on the resulting system for 10 ns (5,000,000 steps), while the results were visualized using VMD and the Biovia discovery studio. A similar procedure was described elsewhere¹⁶. Additionally, MolAICal software was used to compute the ligand-binding affinity by Molecular Mechanics Generalized Born Surface Area (MM/GBSA) method based on the resulting MD log files obtained with NAMD²⁹. MM/GBSA is estimated using **Equations 1 to 3**, where ΔE_{MM} is the gas phase MM energy; $-T\Delta S$ represents the conformational entropy; ΔE_{MM} is the sum of ΔE_{ele} , van der Waals energy ΔE_{vdw} and $\Delta E_{internal}$ of bond, angle, and dihedral energies; ΔG_{sol} is the solvation free energy equal to the sum of the non-electrostatic solvation component ΔG_{SA} and electrostatic solvation energy ΔG_{GB} .

Table II. Parameter settings utilized for the molecular docking simulation

Parameters	Selected option
	Scoring function
Score	MolDock score
Grid resolution	0.30Å
	Binding site
	2HNL
Origin	Volume: 38.912; Surface: 139.52
Center	X: 20.72; Y: 56.17; Z: 24.00
Radius	15
	1TU7
Origin	Volume: 33.28; Surface: 144.64
Center	X: 25.82; Y: 18.62; Z: 18.32
Radius	15
	Search algorithm
Algorithm	MolDock SE
Number of runs	10
Constrain poses to cavity	YES
After docking: Energy minimization	YES
After docking: Optimize H-bonds	YES
	Parameter setting
Maximum iteration	1500
Maximum population size	50
	Pose generation
Energy threshold	100
	Simplex evolution
Maximum steps	300
Neighbor distance factor	1.00
	Multiple poses
The maximum number of poses returned	5
Enable energy threshold	0.00
Cluster similar poses	RMSD threshold: 1.00

$$\Delta G_{bind} = \Delta H - T\Delta S \approx \Delta E_{MM} + \Delta G_{sol} - T\Delta S \quad [1]$$

$$\Delta E_{MM} = \Delta E_{internal} + \Delta E_{ele} + \Delta E_{vdw} \quad [2]$$

$$\Delta G_{sol} = \Delta G_{SA} + \Delta G_{GB} \quad [3]$$

RESULTS AND DISCUSSION

Virtual docking screening

The results (Moldock scores) of the docking simulation conducted between the two receptors of *O. volvulus* and the various benzimidazole-benzoxaborole hybrids, as well as the reference drug (flubendazole), were reported in **Table III**, while **Figure 1** shows the 3D representation of compound **20** in the active sites of both target proteins. The binding score, which indicates the affinity between a ligand and a receptor, is often used to screen an extensive library of compounds to find more active molecules interacting strongly with the receptor of interest. The binding affinities (Moldock scores) available in **Table III** range from -164.682 to -120.466 for 2HNL and -162.699 to -125.359 for 1TU7, with FBZ showing relatively weaker interactions with both receptors (FBZ_2HNL = -120.466 and FBZ_1TU7 = -125.359). The higher binding scores associated

with the hybrids may be attributed to incorporating the benzoxaborole group into the benzimidazole core. The average Moldock scores for the nineteen benzimidazole-benzoxaborole analogs were computed as -148.009 and -144.113 for 2HNL and 1TU7, respectively, and were utilized as cut-offs for selecting the most active analogs. Consequently, seven analogs with Moldock scores equal to or better than the average values were selected alongside FBZ for further evaluation, including compounds **6**, **14**, **15**, **16**, **18**, **19**, and **20**. More so, compound **20** is promising as it binds relatively very strongly with both receptors (characteristic of multi-target drug molecules) while having the highest reported biological activity (pIC_{50}) of 8.3979, the same as that of FBZ. Therefore, the virtual docking screening has proved effective as the most active analogs were identified and extracted for further evaluation.

Table III. Binding interactions affinities (MolDock scores) of FBZ and the various benzimidazole-benzoxaborole hybrids with 2HNL and 1TU7

ID	MolDock score	
	2HNL	1TU7
1*	-120.466	-125.359
2	-139.139	-139.513
3	-139.071	-135.771
4	-142.442	-138.948
5	-146.906	-136.352
6	-147.636	-146.873
7	-141.533	-141.555
8	-142.674	-139.775
9	-151.243	-139.614
10	-149.539	-138.977
11	-149.757	-140.454
12	-139.11	-142.526
13	-151.728	-137.262
14	-155.19	-143.315
15	-152.069	-148.999
16	-164.682	-147.688
17	-144.272	-148.61
18	-151.502	-151.512
19	-149.652	-162.699
20	-154.024	-157.696

Note: 1* - Flubendazole (FBZ)

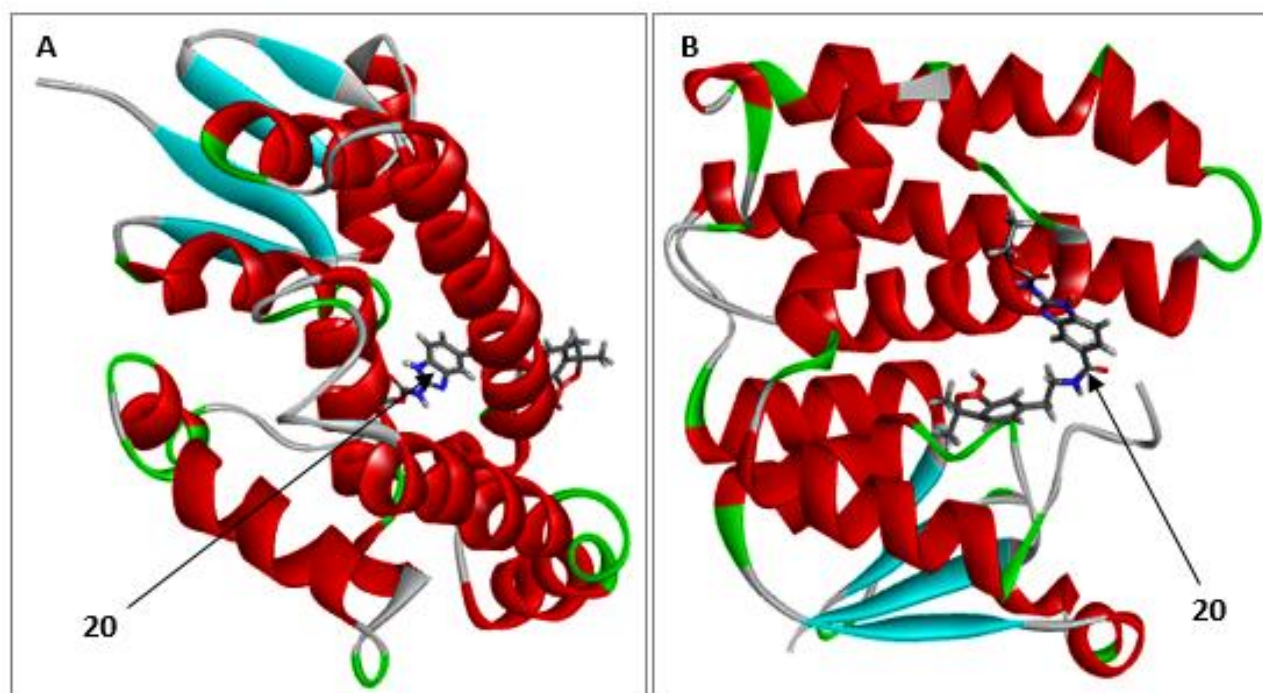


Figure 1. 3D representation of compound **20** in the active site of (A) prostaglandin D synthase (PDB: 2HNL) (B) Pi-class Glutathione S-transferase (PDB: 1TU7)

Evaluation of pharmacokinetic properties

Drug-likeness analysis and ADMET studies were conducted on FBZ and the seven selected analogs (**6**, **14**, **15**, **16**, **18**, **19**, and **20**) to ascertain their oral bioavailability, toxicity, and safety profiles. The results of both investigations were presented in **Tables IV** and **V**, respectively, with **Figures 2** and **3** showing the bioavailability radar, while **Figure 4** showed their Boiled Egg's representation. Lipinski's approach to ascertaining the oral bioavailability of compounds has been widely applied in the discovery of new drug molecules¹³. It asserts that a drug molecule may likely not be bioavailable orally when it has an HBD greater than 5, HBA > 10, MW > 500, and MLOGP > 4.15 or WLOGP > 5¹⁵. Whenever a molecule passes at least three of the four provisions of the RO5, it is said to comply with Lipinski's rule for oral bioavailability¹⁴. **Table IV** shows that FBZ and all the tested benzimidazole-benzoxaborole analogs passed the drug-likeness test (Lipinski RO5) by showing no violation. The reported Topological Polar Surface Area (TPSA) values for the molecules were below the threshold value of 140 Å², beyond which a molecule may exhibit poor Human Intestinal Absorption (HIA). Also, the synthetic accessibility (SA) scores of these compounds were less than 5.00 (accessible portion on a scale of 1 to 10), suggesting easy laboratory synthesis of these molecules. The predicted values of the estimated water solubility (Log S) range of $-2 > \text{Log S} > -4$ indicate that these molecules are aqueous soluble. None of the compounds were also predicted as Pan Assay Interference compounds (PAINS).

The estimated ADMET properties reported in **Table V** showed good Human Intestinal Absorption (HIA) (greater than 65%) for all tested compounds. Skin permeability is a key factor in transdermal drug delivery development, with skin permeation constant LogKp > -2.50 indicating poor skin permeability. As a result, the various compounds showed LogKp values < -2.50, connoting good skin permeability. Drug molecule penetration through the Blood-Brain Barrier (BBB) and Central Nervous System (CNS) comes with specific criteria, which specify that for a drug molecule to penetrate the BBB and CNS readily, the logarithmic ratio of brain-to-plasma drug concentration (logBB) must be > 0.3 and the blood-brain permeability-surface area product (logPS) be > -2 respectively. Consequently, none of these molecules were predicted to penetrate the BBB and CNS readily.

Furthermore, some groups of cytochromes P450 enzymes are important in the body to facilitate drug metabolism and help in their excretion. The two major isoforms enhancing drug metabolism, CYP3A4 and CYP2D6, were tested. However, the tested molecules were not substrates and inhibitors of both enzymes. Also, FBZ only is a non-substrate of P-glycoprotein, an enzyme that acts as a biological barrier by extruding toxins and xenobiotics, including drugs, out of cells. This means that FBZ may not be effluated out of the target cells by this enzyme when taken into the human system. However, like FBZ, only **6**, **14**, and **20** showed inhibition of this enzyme. The drug's total clearance determines the extent of drug removal from the body. The range of total clearance values for all the tested molecules is good. The renal Organic Cation Transporter 2 (OCT2) is critical in drug and endogenous compounds' disposition and renal clearance. However, the activities of OCT2 may cause unwanted drug-drug interactions, which makes it necessary to ascertain whether a drug molecule is an OCT2 substrate or inhibitor. As seen in **Table V**, all the tested compounds are non-OCT2 substrates.

Additionally, some toxicity indices were predicted to ascertain the safety profiles of these molecules. The Ames test is widely applied to ascertain a compound's mutagenic potential. A positive test indicates that the compound is mutagenic. Only compounds **6**, **15**, and **18** showed positive Ames toxicity, showing a mutagenicity risk. Also available in **Table V** is the Maximum Recommended Tolerated Dose (MRTD) predicted for the various molecules. MRTD value of $\leq 0.477 \log (\text{mg}/\text{kg}/\text{day})$ is considered low, while a value $> 0.477 \log (\text{mg}/\text{kg}/\text{day})$ is considered high. The inhibition of the human ether-a-go-go gene (hERG) is responsible for the acquired long QT syndrome, resulting in heartbeat irregularity issues. Only FBZ was implicated in this regard. Furthermore, all the tested compounds showed positive hepatotoxicity but negative skin sensitization, eye irritation, and carcinogenicity. Additionally, only FBZ and compound **6** are nephrotoxic, indicating the risk of rapid deterioration in kidney function.

Based on the toxicity analysis, compounds **14**, **16**, **19**, and **20** exhibited relatively safer toxicity profiles. Therefore, further evaluations were limited to these molecules and FBZ. The bioavailability radar displayed in **Figures 2** and **3** was to provide a rapid appraisal of the molecules' drug-likeness. The radar considers six physicochemical properties: size, polarity, lipophilicity, solubility, flexibility, and saturation. The radar's pink area represents the ideal or suitable physicochemical space in which the molecule falls completely to be classified as drug-like. This means lipophilicity ($-0.7 \leq \text{XLOGP3} \leq +5.0$), size ($150 \leq \text{MW} \leq 500$), polarity ($20 \leq \text{TPSA} \leq 130$), solubility ($\text{Log S} \leq 6$), saturation (fraction of carbons in the sp³ hybridization ≥ 0.25), and flexibility (No. of rotatable bonds ≤ 9)²². The selected molecules (**14**, **16**, **19**, and **20**) were said to be orally

bioavailable, as seen from their bioavailability radar in **Figure 2**. FBZ, on the other hand, showed high unsaturation due to its low fraction of carbon in the sp³ hybridization and, therefore, is not orally bioavailable. This conforms with reports available in the literature regarding the need to improve the oral bioavailability of FBZ⁸. **Figure 4** shows the boiled egg representation of FBZ and the four molecules of benzimidazole-benzoxaborole analogs. All the molecules were located in the boiled egg's white, indicating that they were predicted to be passively absorbed by the gastrointestinal tract. Also, only the reference drug appeared in the red dot, showing that it was predicted not to be effluated from the CNS by the p-glycoprotein. The four compounds' overall drug-likeness and ADMET properties (**14**, **16**, **19**, and **20**) showed better pharmacokinetic profiles than the reference drug, especially in bioavailability and toxicity.

Table IV. Predicted drug-likeness properties of FBZ and some selected benzimidazole-benzoxaborole hybrids

Properties	FBZ	Selected compounds						
		6	14	15	16	18	19	20
Molecular weight	313.28	379.17	407.23	380.16	422.24	394.19	422.24	436.27
TPSA	84.08	113.54	113.54	125.57	125.57	125.57	125.57	125.57
MLOGP	2.07	0.81	1.26	0.74	1.15	0.70	1.15	1.37
WLOGP	3.34	1.63	2.21	1.07	1.56	0.78	1.56	1.76
XLOGP3	2.84	2.35	2.58	1.62	2.14	1.55	2.14	2.60
Fraction Csp ³	0.06	0.21	0.29	0.17	0.29	0.21	0.29	0.32
Estimated solubility, LogS	-3.72	-3.74	-3.9	-3.15	-3.64	-3.12	-3.64	-3.94
Synthetic accessibility	2.30	3.44	3.55	3.33	3.61	3.44	3.56	3.70
No. of rotatable bonds	5	5	7	7	8	8	8	9
No. of H-bond acceptors	5	6	6	6	6	6	6	6
No. of H-bond donors	2	3	3	4	4	4	4	4
PAINS	0	0	0	0	0	0	0	0
Lipinski violation	0	0	0	0	0	0	0	0
Drug-likeness	YES	YES	YES	YES	YES	YES	YES	YES

Table V. Predicted ADMET properties of FBZ and some selected benzimidazole-benzoxaborole hybrids

ADMET properties	FBZ	Selected compounds						
		6	14	15	16	18	19	20
Absorption								
Human Intestinal Absorption (%)	88.62	79.89	77.60	74.84	70.63	69.34	67.66	66.85
Skin permeability	-2.74	-2.74	-2.74	-2.74	-2.74	-2.74	-2.74	-2.74
P-glycoprotein substrate	NO	YES	YES	YES	YES	YES	YES	YES
P-glycoprotein I inhibitor	YES	NO	YES	NO	NO	NO	NO	NO
P-glycoprotein II inhibitor	YES	YES	YES	NO	NO	NO	NO	YES
Distribution								
BBB permeability (LogBB)	-1.112	-1.143	-1.073	-1.140	-1.073	-1.056	-1.131	-1.054
CNS permeability (LogPS)	-2.469	-3.579	-3.430	-3.709	-3.613	-3.759	-3.613	-3.599
Metabolism								
CYP2D6 substrate	NO	NO	NO	NO	NO	NO	NO	NO
CYP3A4 substrate	NO	NO	NO	NO	NO	NO	NO	NO
CYP2D6 inhibitor	NO	NO	NO	NO	NO	NO	NO	NO
CYP3A4 inhibitor	NO	NO	NO	NO	NO	NO	NO	NO
Excretion								
Total clearance (Log ml/min/kg)	0.825	0.993	1.102	1.061	1.015	1.108	1.021	1.028
Renal OCT2 substrate	NO	NO	NO	NO	NO	NO	NO	NO
Toxicity								
AMES Toxicity	NO	YES	NO	YES	NO	YES	NO	NO
Max. tolerated dose (Log mg/kg/day)	0.254	0.36	0.349	0.377	0.44	0.398	0.435	0.426
hERG inhibitor	YES	NO	NO	NO	NO	NO	NO	NO
Hepatotoxicity	YES	YES	YES	YES	YES	YES	YES	YES
Skin sensitization	NO	NO	NO	NO	NO	NO	NO	NO
Eye irritation	NO	NO	NO	NO	NO	NO	NO	NO
Carcinogenicity	NO	NO	NO	NO	NO	NO	NO	NO
Nephrotoxicity	YES	YES	NO	NO	NO	NO	NO	NO

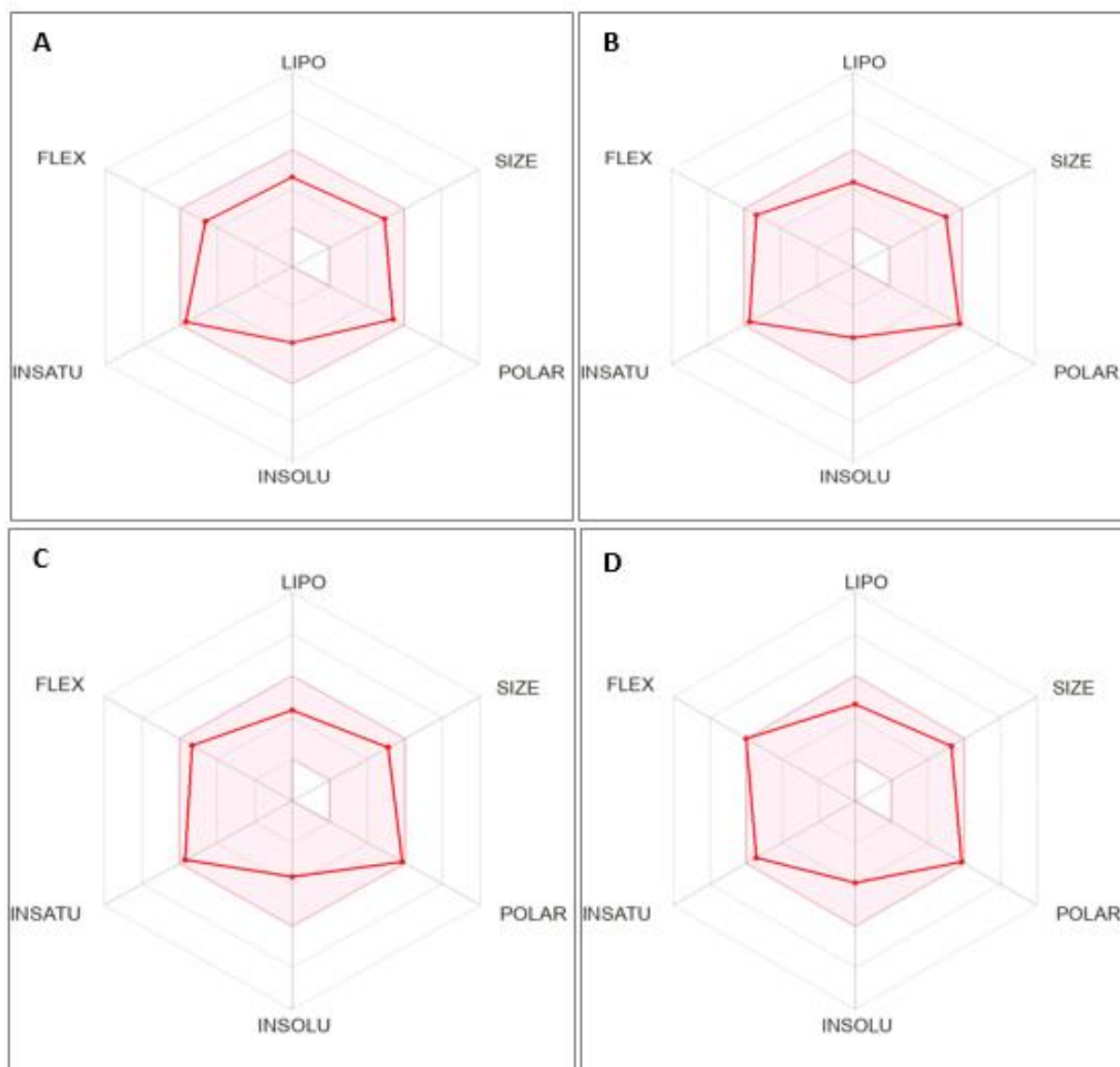


Figure 2. Oral bioavailability radar of (A) Compound 14 (B) Compound 16 (C) Compound 19, and (D) Compound 20

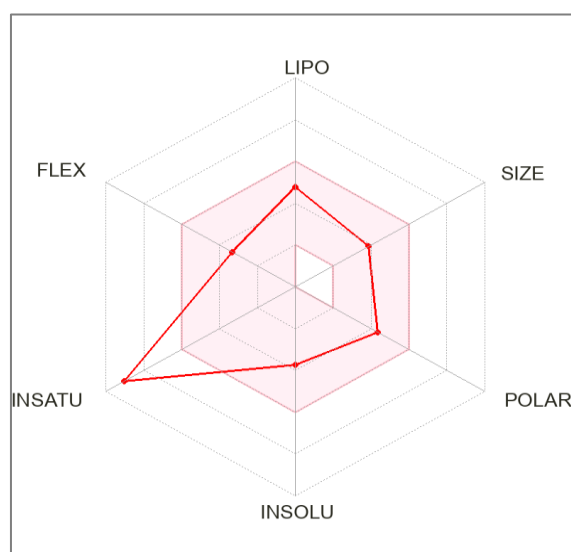


Figure 3. Oral bioavailability radar of FBZ

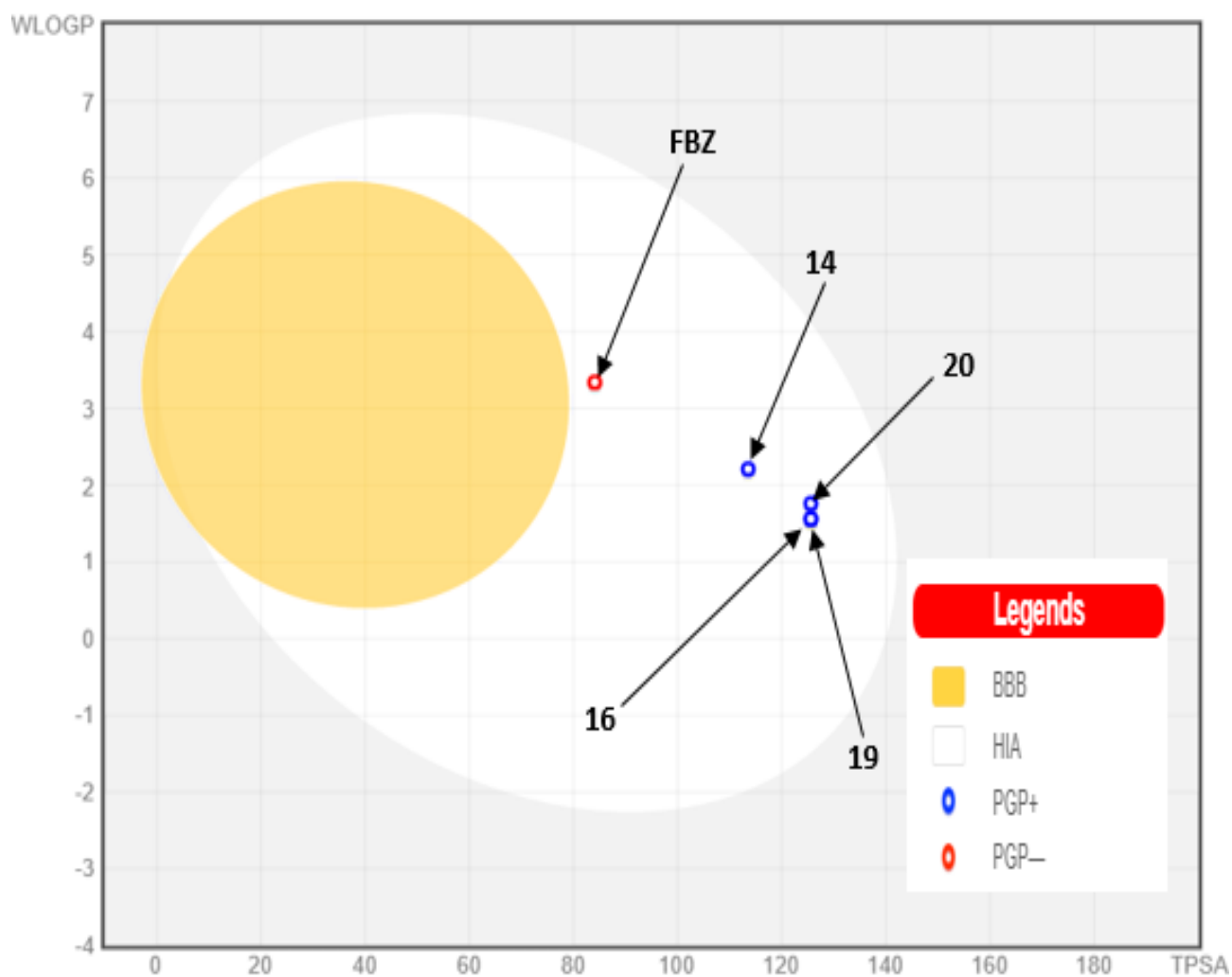


Figure 4. The Boiled-Egg representation of FBZ and the selected benzoxaborole analogs

Pharmacological interactions

The pharmacological interactions between the receptors' amino acid residues and the selected compounds (**14**, **16**, **19**, and **20**), as well as the reference drug (FBZ), were summarized in **Table VI**, while the 2D and 3D views of the binding interactions as adapted from the Discovery Studio Visualizer were shown in **Figures 5 to 14**. This was to provide insight into the mode of binding of these ligands with the active sites of the various target proteins. The various compounds were said to interact adequately with the respective target receptors, as shown by the presence of hydrogen bonding (H-bond), electrostatic interactions, and hydrophobic interactions (**Table VI**). H-bonding and hydrophobic interactions were present in all the interactions involving the two target proteins, while electrostatic interactions were more visible in the interactions involving 1TU7 than in those of 2HNL. Incorporating the benzoxaborole group into the benzimidazole core significantly improved the binding interactions of the selected analogs with the receptors, as seen in the higher binding affinities associated with these molecules. Because compound **20** interacted very strongly with both receptors (Moldock score= -154.024 for 2HNL and -157.696 for 1TU7) and also had the highest pIC₅₀ value of 8.3979, its binding interactions were discussed and compared with those of the reference drug (FBZ).

A total of two conventional H-bonds, two carbon H-bonds, two π -anion electrostatic interactions, and up to eight hydrophobic interactions were formed between compound **20** and 1TU7 (**Figure 12**). Both the benzoxaborole and benzimidazole groups were involved in the interactions. The conventional H-bonds were formed between VAL-200 and the amide linker at a distance of 1.81 Å and between LYS-183 and the oxygen hetero atom of the benzoxaborole group at a distance of 2.01 Å. The carbon H-bonds were formed with ILE-163 and ARG-195 at a distance of 2.71 and 2.85 Å, respectively. The π -electron systems of the benzene ring present in both groups were helpful in the formation of π -anion electrostatic interactions with ASP-159 at a distance of 4.37 Å and ASP-196 at distances of 3.62 and 3.66 Å. The hydrophobic interactions

include Amide π -stacked with ARG-195, Alkyl interactions with CYS-192, LYS-183, and ILE-163, and π -alkyl interactions with LYS-199, ILE-163, and ARG-195. An unfavorable steric bump was visible with LYS-183.

On the other hand, the binding interaction profile of FBZ with 1TU7 involved four conventional H-bond interactions, two π -cation and two π -anion electrostatic interactions, and up to five hydrophobic interactions (**Figure 14**). Unlike in 20_1TU7, no unfavorable steric clash was visible. The conventional H-bonds were formed with ARG-195 at a distance of 3.10 Å, LYS-183 (2.33Å), and VAL-200 at distances of 2.20 and 2.89 Å. Also visible were π -cation electrostatic interactions with ARG-11 and LYS-183 at distances of 3.69 and 3.59 Å respectively, and π -anion electrostatic interactions with ASP-159 and ASP-196 at 3.76 and 3.73 Å respectively. The hydrophobic interactions include Amide π -stacked with ARG-195, alkyl interaction with LYS-199, and π -alkyl interactions with ARG-195, ILE-163, and CYS-192.

The binding interactions of both compounds with 2HNL, unlike that with 1TU7, lacked electrostatic interactions. Comparing the binding profiles 20 with FBZ revealed a significant similarity in their binding mode with both receptors. Although both compounds showed more remarkable similarity in their binding pattern, their binding scores differ significantly. This may be attributed to the variations in the strength of their interactions and the contributions of Van der Waals interactions which were not visible.

Table VI. Summary of predicted binding interaction profiles of **14**, **16**, **19**, and **20** with 2HNL and 1TU7

ID	Hydrogen bond Interactions			Electrostatic/Hydrophobic interactions
	Amino acid	Type	Distance (Å)	
FBZ_2HNL	ARG-38	Conventional	2.30	TYR-32 (π - π Stacked), HIS-131 (π - π T-shaped), PRO-76 (Alkyl), ILE-127 (π -alkyl)
	VAL-75	Conventional	1.91	
14_2HNL	ARG-38	C - H	2.85, 2.95	HIS-131 (π - π T-shaped), Alkyl (MET-186, VAL-75), π -alkyl (ARG-36, TYR-32, PHE-33), THR-187 (π -lone pair)
	ASN-183	Conventional	1.77, 2.79	
	ARG-220	Conventional	2.78, 2.79	
	THR-187	C - H	2.65	
16_2HNL	ARG-36	π -donor	2.37	π - π T-shaped (HIS-131, PHE-123), π -alkyl (HIS-131, PHE-225, PHE-123, PHE-33, TYR-32, HIS-89, MET-184), and unfavorable steric bumps with MET-184
	ASN-183	Conventional	2.20	
	ARG-36	Conventional	3.00	
19_2HNL	PHE-225	C - H	2.56	GLU-87 (π -anion), π -cation (ARG-38, ARG-60), HIS-74 (π - π T-shaped), HIS-74 (π - π stacked), LYS-67 (π -alkyl), and unfavorable donor-donor clash with TRP-63
	LYS-67	Conventional	2.10, 2.40	
	TYR-32	Conventional	2.50	
	SER-88	Conventional	1.91	
20_2HNL	VAL-75	C - H	2.95	PHE-123 (π - π stacked), π - π T-shaped (HIS-74, HIS-131), LYS-67 (Alkyl), π -alkyl (PHE-123, ILE-127, PHE-33, HIS-74, TRP-63)
	ARG-36	Conventional	2.74	
	THR-187	C - H	2.72	
FBZ_1TU7	ARG-195	Conventional	3.10	π -cation (ARG-11, LYS-183), π -anion (ASP-159, ASP-196), ARG-195 (Amide π -stacked), LYS-199 (Alkyl), π -alkyl (ARG-195, ILE-163, CYS-192)
	LYS-183	Conventional	2.33	
14_1TU7	VAL-200	Conventional	2.20, 2.89	π -anion (ASP-159, ASP-196), Alkyl (LYS-199, PRO-166), π -alkyl (ILE-163, LYS-199)
	ARG-195	Conventional	1.83, 2.57	
	LYS-199	Conventional	1.79	
	GLN-162	Conventional	2.19	
16_1TU7	GLN-162	C - H	2.61	ARG-11 (π -cation), π -anion (ASP-159, ASP-196), ARG-195 (Amide π -stacked), Alkyl (CYS-192, LYS-183, ILE-163), π -alkyl (HIS-179, ARG-195, ILE-163)
	LYS-183	Conventional	2.35, 2.58	
	ILE-163	Conventional	2.71	
	LYS-199	C - H	3.01	
19_1TU7	GLN-162	C - H	2.38	ARG-11 (π -cation), ASP-196 (π -anion), ILE-163 (Alkyl), π -alkyl (ARG-195, ILE-63)
	CYS-192	Conventional	2.06	
	ARG-195	Conventional	2.04, 1.86	
	ILE-163	Conventional	2.86	
	LYS-199	C - H	2.33	
20_1TU7	GLN-162	C - H	2.40	π -anion (ASP-159, ASP-196), ARG-195 (Amide π -stacked), Alkyl (CYS-192, LYS-183, ILE-163), π -alkyl (LYS-199, ILE-163, ARG-195), and unfavorable steric bump with LYS-183.
	ASP-159	C - H	2.86	
	LYS-183	Conventional	2.01	
	VAL-200	Conventional	1.81	
	ARG-195	C - H	2.85	
	ILE-163	C - H	2.71	

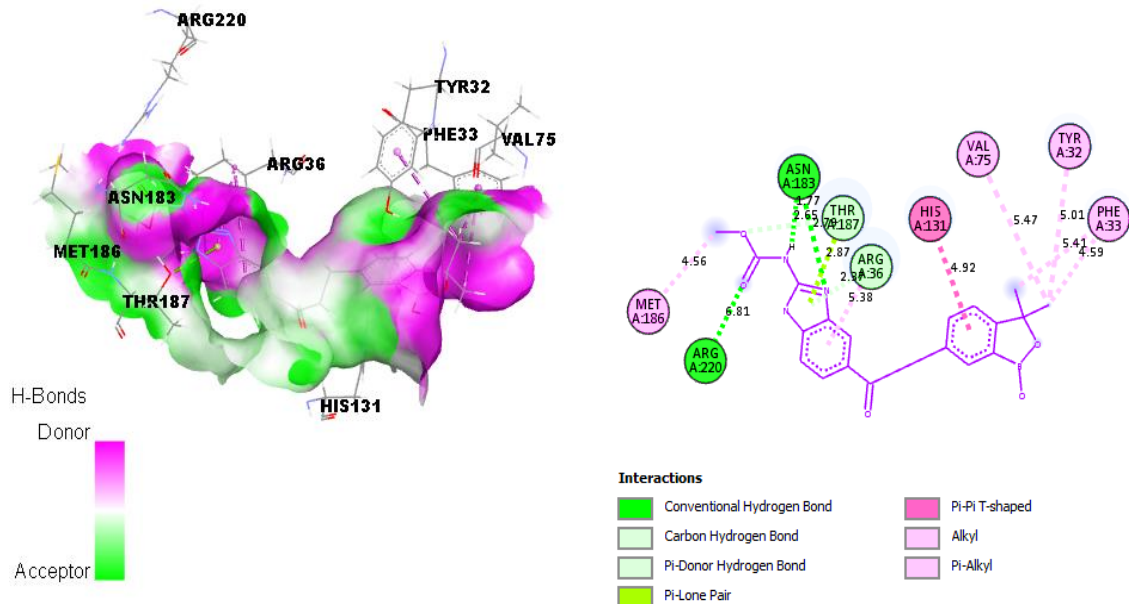


Figure 5. Binding interaction between 14 and Prostaglandin D synthase (PDB: 2HNL)

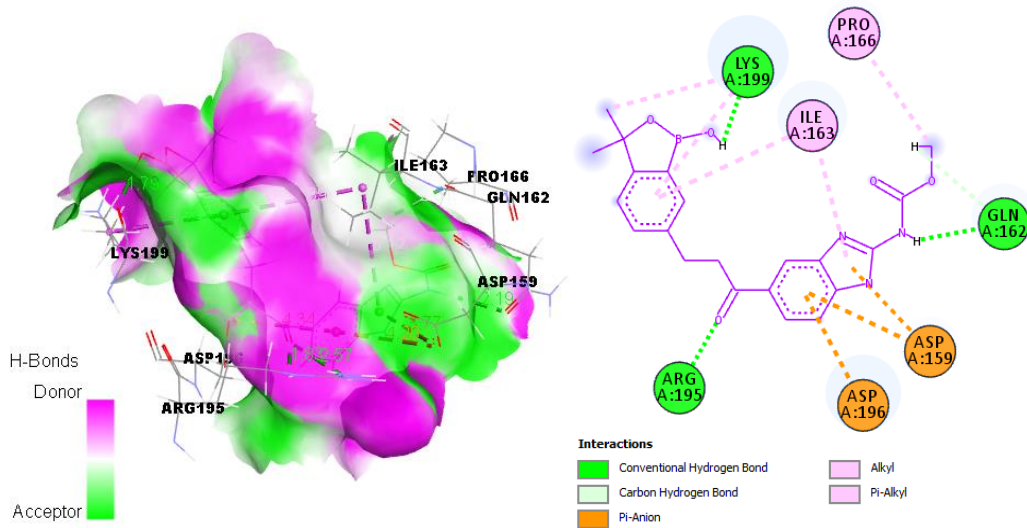


Figure 6. Binding interaction between 14 and Pi-class Glutathione S-transferase (PDB: 1TU7)

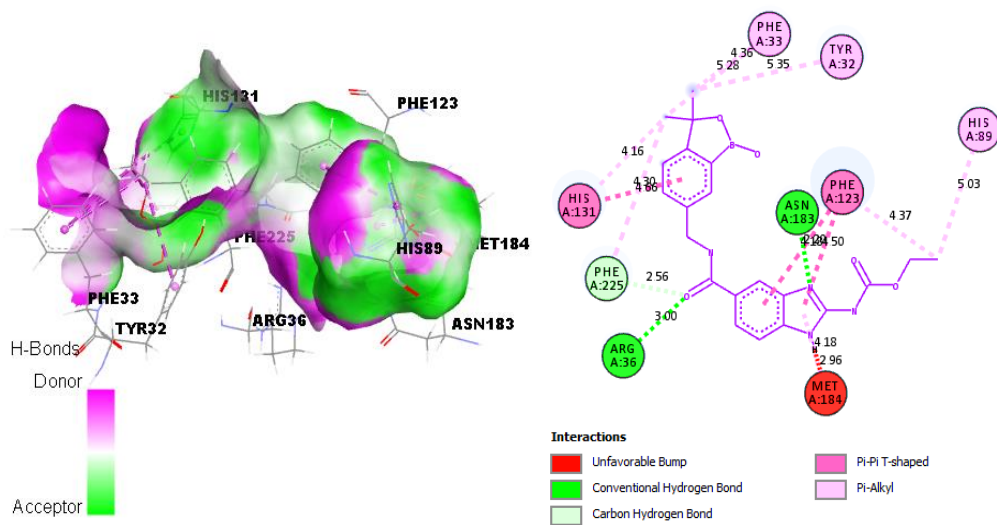


Figure 7. Binding interaction between 16 and Prostaglandin D synthase (PDB: 2HNL)

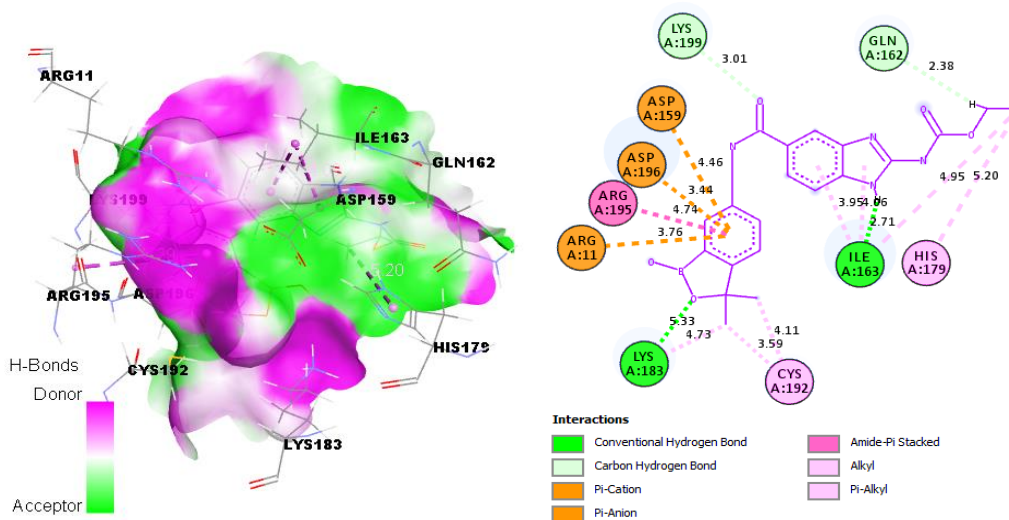


Figure 8. Binding interaction between 16 and Pi-class Glutathione S-transferase (PDB: 1TU7)

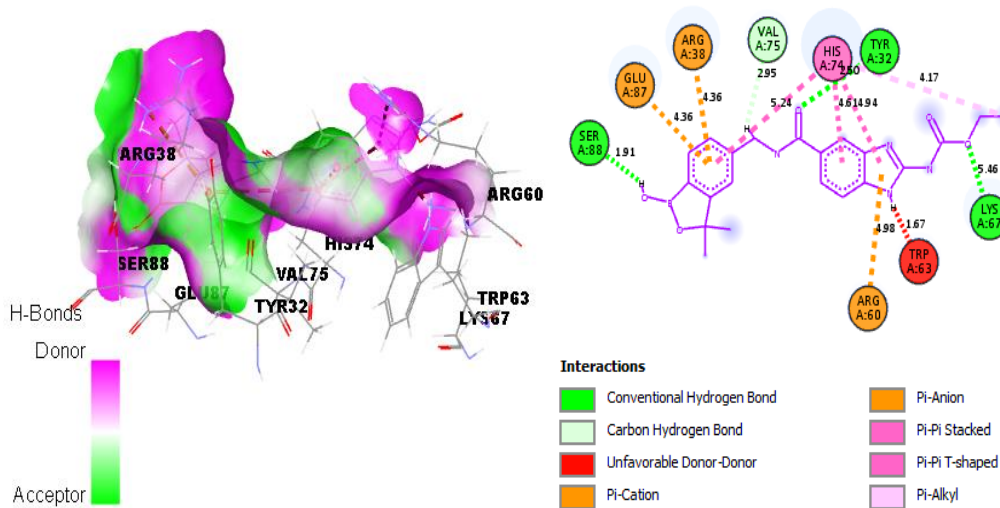


Figure 9. Binding interaction between 19 and Prostaglandin D synthase (PDB: 2HNL)

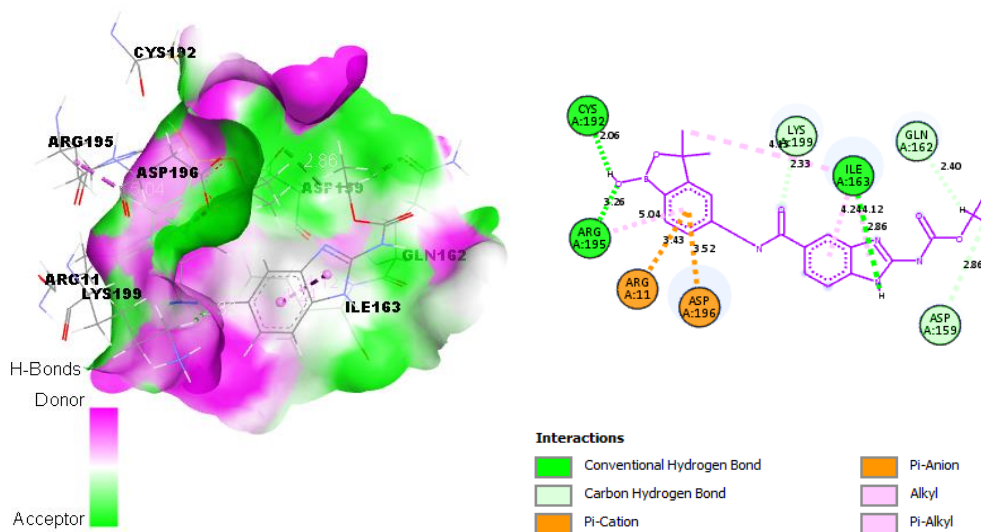


Figure 10. Binding interaction between 19 and Pi-class Glutathione S-transferase (PDB: 1TU7)

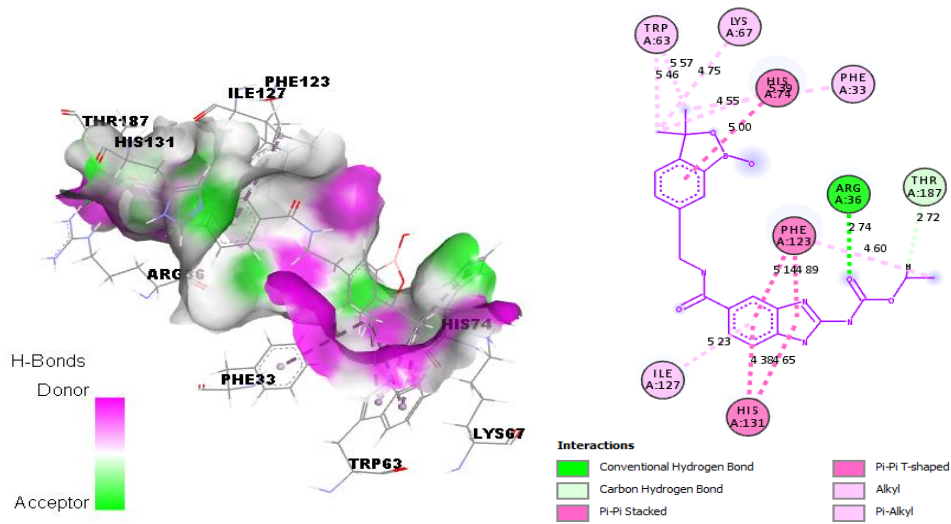


Figure 11. Binding interaction between 20 and Prostaglandin D synthase (PDB: 2HNL)

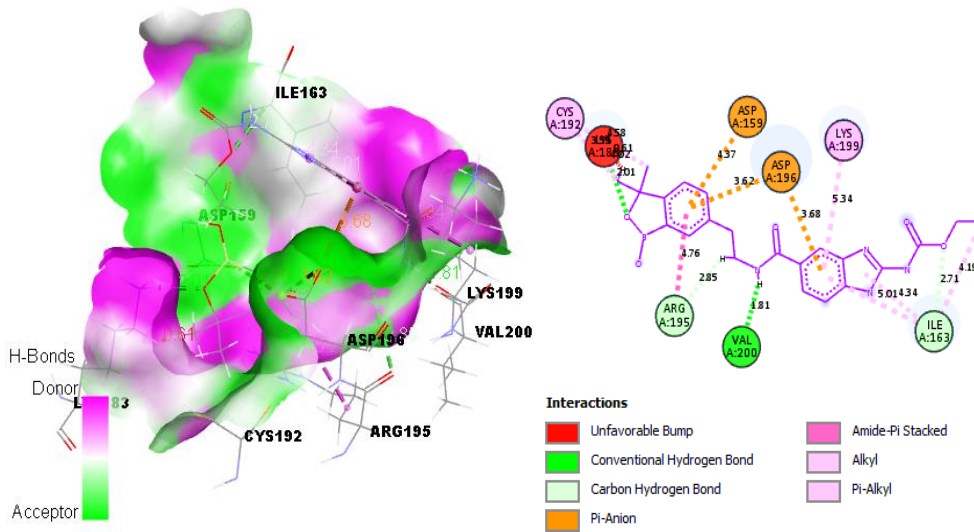


Figure 12. Binding interaction between 20 and Pi-class Glutathione S-transferase (PDB: 1TU7)

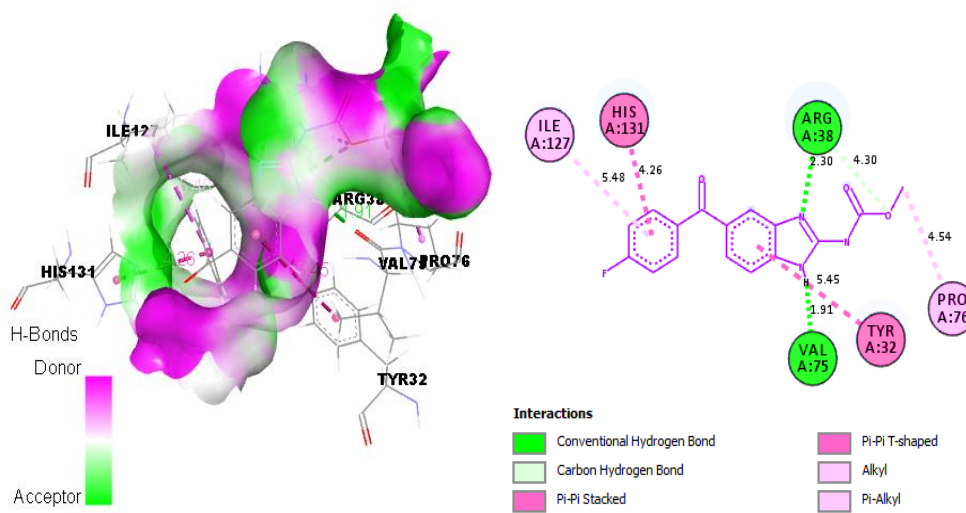


Figure 13. Binding interaction between FBZ and Prostaglandin D synthase (PDB: 2HNL)

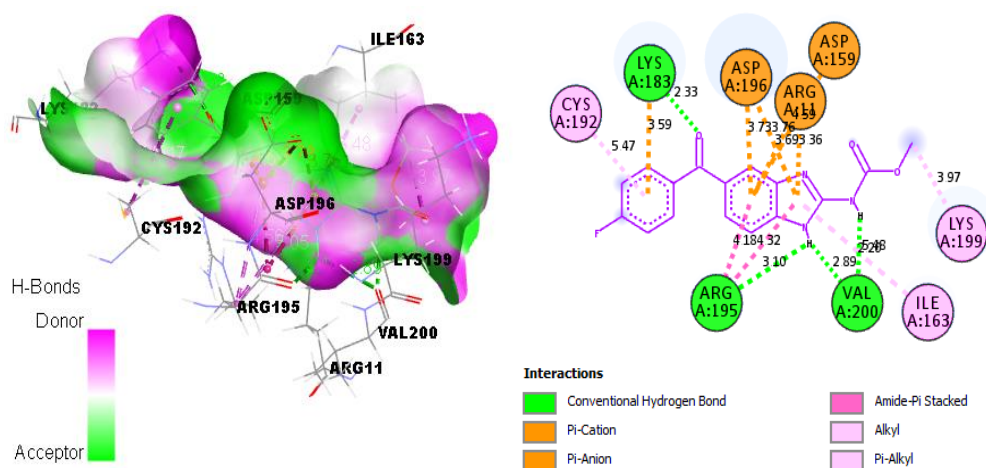


Figure 14. Binding interaction between FBZ and Pi-class Glutathione S-transferase (PDB: 1TU7)

Molecular dynamic study

The complexes of compound **20** with both receptors were subjected to MD simulation to ascertain the stability of the protein-ligand interactions. The results of the simulation, summarized as plots of Root-Mean-Square Deviation (RMSD), Root-Mean-Square Fluctuation (RMSF), and Radius of gyration (Rg) versus the time in nanoseconds (ns), were presented in **Figures 15 to 17**. Also, the result of binding free energy (MM/GBSA) estimated for 20_1TU7 and 20_2HNL by MolAICal is shown in **Table VII**. In addition, the 3D structural orientations of compound **20** in the active sites of both receptors before and after MD simulation were presented in **Figures 18 and 19** for 1TU7 and 2HNL, respectively. Furthermore, the 2D views of the resulting binding interactions of the complexes before and after the MD simulation was shown in **Figures 20 and 21** for 20_1TU7 and 20_2HNL, respectively.

The overall average RMSD values were estimated as 9.4609 and 11.8643 Å for 20_1TU7 and 20_2HNL, respectively. **Figure 15** shows that 20_2HNL deviated significantly (21.3988 Å) at the start of the simulation and fell gently as the simulation progressed, reaching equilibrium at 10 ns (0.0000 Å). For 20_1TU7, the RMSD increased gradually from 0.0000 Å at the start of the simulation and reached the peak (17.8253 Å) at 5.5 ns, after which it fell to 4.6270 Å at 10 ns. The RMSF is more like a calculation of the flexibility or the extent of movement of individual residue during a simulation. The RMSF plots in **Figure 16** showed that the protein residues were slightly flexible between 0.5 and 1 Å during the trajectory, indicating the stable proteins during the simulation³⁰. The Rg measures the degree of a protein's compactness during the trajectory. Decreasing Rg indicates reducing residues' flexibilities and more stability for the protein. The variations of Rg from the start to the end of the simulation were 0.60 and 0.52 Å for 1TU7 and 2HNL, respectively (**Figure 17**), connoting slight changes in the protein compactness as the simulation progresses, which therefore means both complexes could be stable.

Furthermore, the result of binding free energy (MM/GBSA) estimated for 20_1TU7 and 20_2HNL (**Table VII**) shows that 20_1TU7 has a positive free energy value (+320.7898 kcal/mol) while 20_2HNL has a negative value of -29.6742 kcal/mol. This shows that the binding interactions of compound **20** with 2HNL are favorable, energetically stable, and bind strongly with the receptor. A similar observation was reported elsewhere for binding free energy change (MM/GBSA) calculated for some analogs of 2-aryl benzimidazole in a complex with PdxK³¹. Additionally, the orientations of compound **20** in the active sites of both receptors before and after the MD simulation was shown in **Figures 18 to 19**, which showed a slight change in the position of compound **20** on 2HNL after the simulation (**Figure 19B**). However, the position of the compound on 1TU7 appeared to be reversed, curving away from the receptor's active site after the simulation (**Figure 18B**). **Figures 20 and 21** presented the resulting binding interactions for 20_1TU7 and 20_2HNL, respectively. From **Figure 20B**, no interactions were visible between compound **20** and 1TU7, which could be attributed to the reversed position of the compound on the receptor after the MD simulation. From **Figure 21B**, on the other hand, none of the previous interactions was retained, though new interactions were formed, including one conventional Hydrogen bond with ARG-60 at a distance of 1.93 Å, and two carbon-hydrogen bonds with PHE-123 at 2.94 and 3.00 Å. Others are two electrostatic bonds, one π -cation with ARG-60 at 3.66 Å and one π -anion with PHE-225 at 4.40 Å, and one hydrophobic interaction (π - π stacked) with PHE-225 at a distance of 4.44 Å. Therefore, Prostaglandin D synthase (2HNL) is confirmed as a promising therapeutic target for benzoxaborole-benzimidazole hybrids.

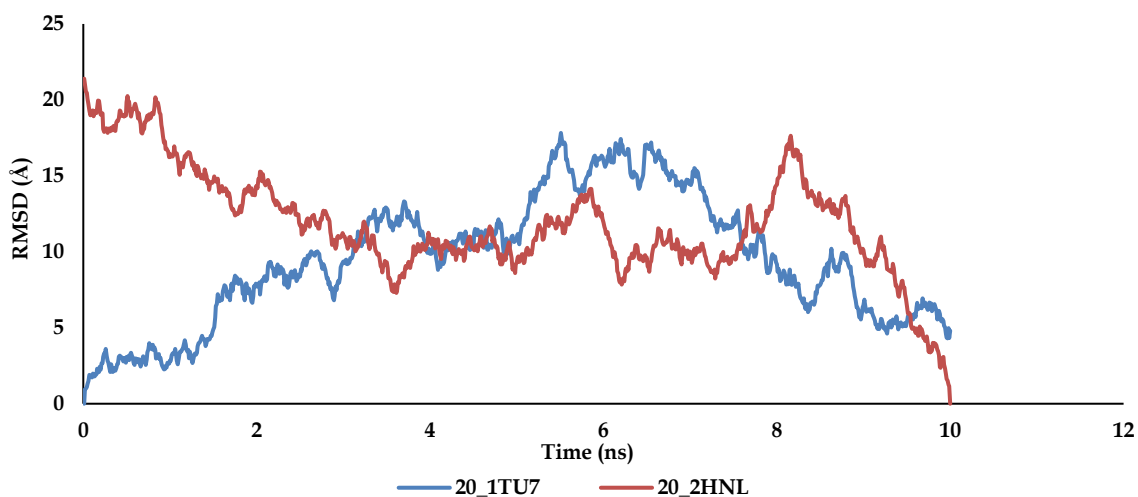


Figure 15. RMSD plot for MD simulation of Compound 20 with 1TU7 and 2HNL

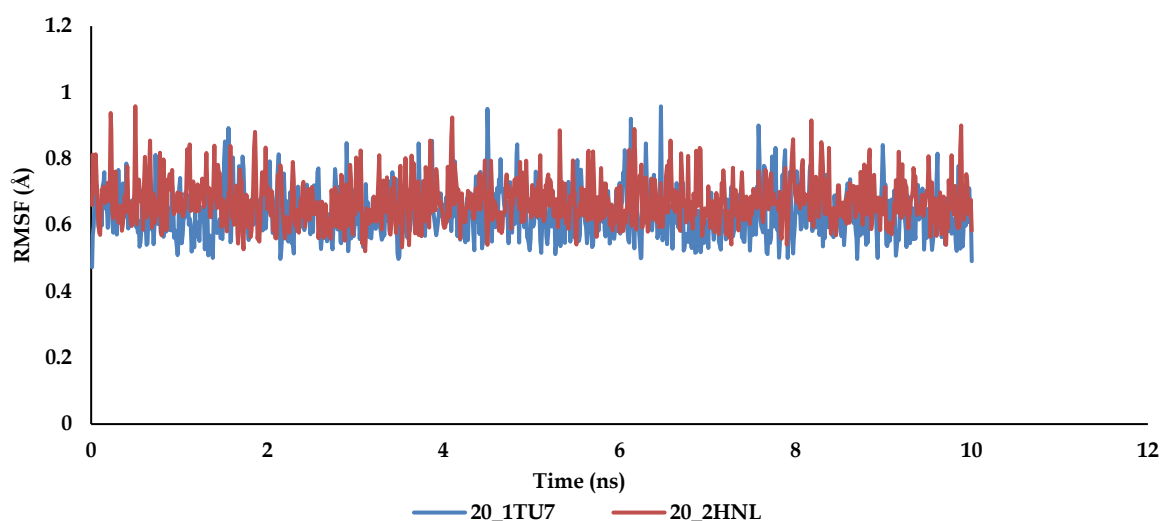


Figure 16. RMSF plot for MD simulation of Compound 20 with 1TU7 and 2HNL

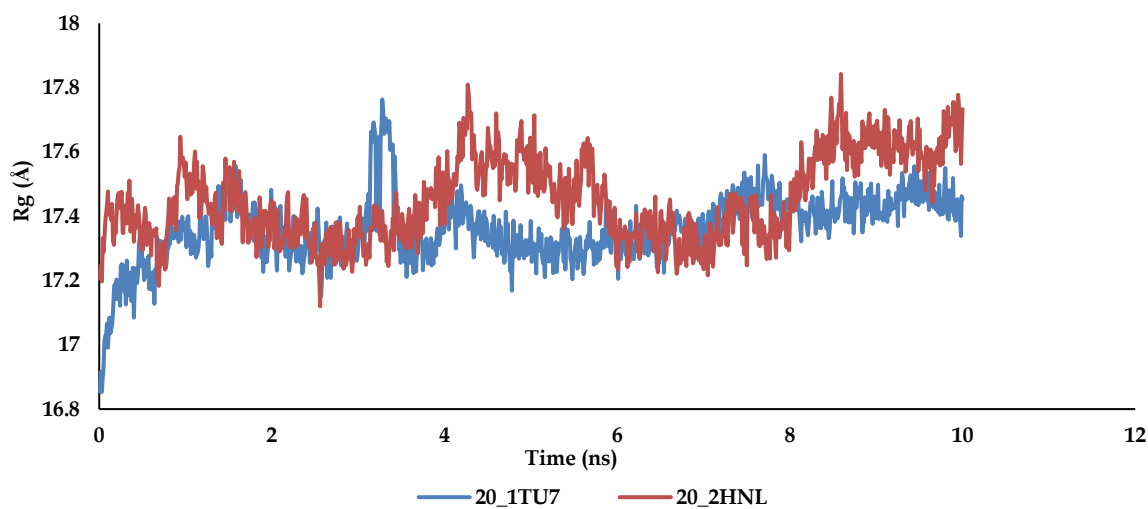


Figure 17. Plot of Rg versus time for MD simulation of Compound 20 with 1TU7 and 2HNL

Table VII. Binding free energy parameters of 20_1TU7 and 20_2HNL complexes

Energy (kcal/mol)	20_1TU7	20_2HNL
$\Delta E(\text{internal})$	16.6886	19.7066
$\Delta E(\text{electrostatic}) + \Delta G(\text{solvation})$	-0.7552	-15.6184
$\Delta E(\text{Van der Waals})$	304.8563	-33.7624
$\Delta G_{\text{binding}}(\text{MM/GBSA})$	+320.7898	-29.6742

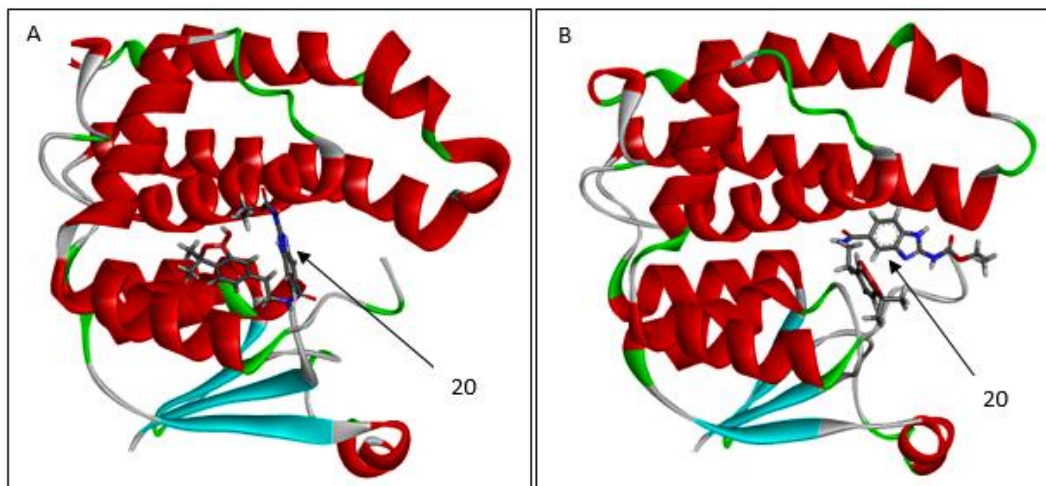


Figure 18. 3D structural orientation of 20_1TU7 (A) before and (B) after MD simulation

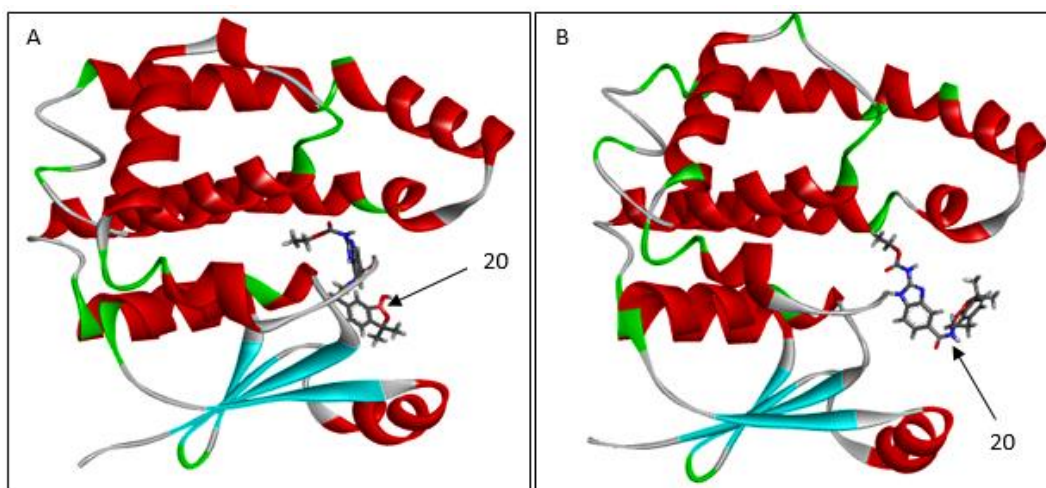


Figure 19. 3D structural orientation of 20_2HNL (A) before and (B) after MD simulation

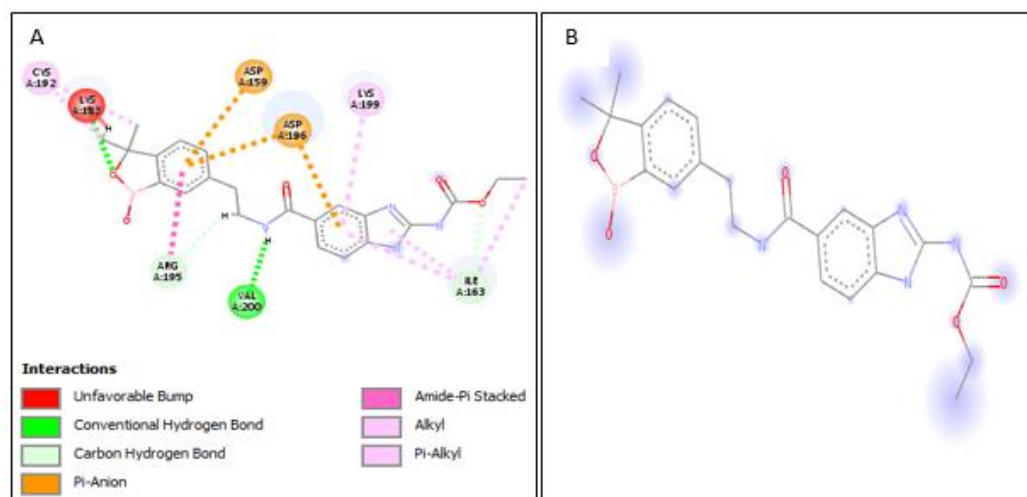


Figure 20. 2D representation of binding interactions of 20_1TU7 (A) before and (B) after MD simulation

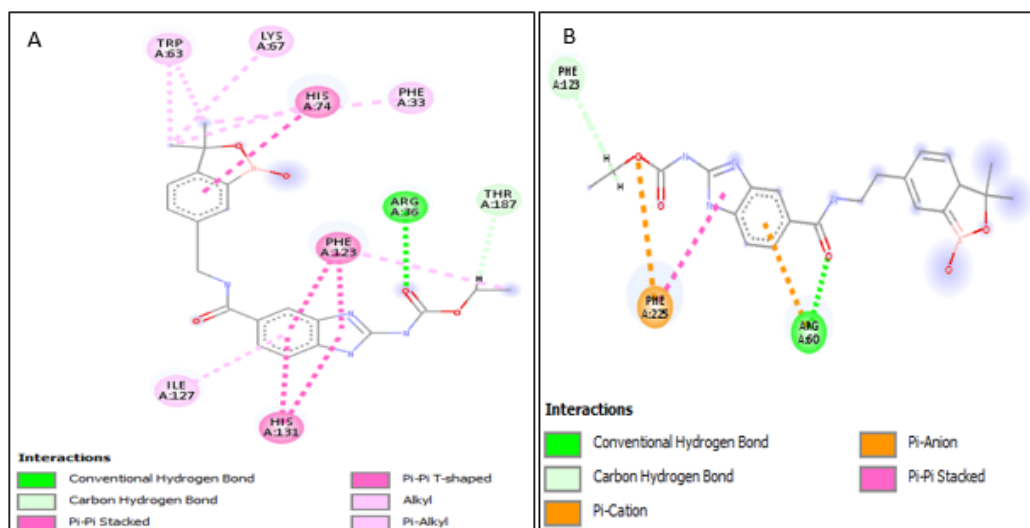


Figure 21. 2D representation of binding interactions of 20_2HNL (A) before and (B) after MD simulation

CONCLUSION

The combined molecular docking screening and pharmacokinetics approach identified four benzimidazole-benzoxaborole analogs (**14**, **16**, **19**, and **20**) as the most active molecules forming high binding affinities with the two protein receptors (2HNL and 1TU7). These molecules were predicted to be orally bioavailable, less toxic, and possessed better pharmacokinetic profiles than the reference compound (FBZ). These compounds' predicted pharmacological interaction profiles and FBZ generally fit well into the target site cavities. Compound **20** showed a typical characteristic of a multi-target drug molecule as it binds energetically stronger with both targets than other analogs. Additionally, the MD simulation revealed the stability of the interactions between compound **20** and 2HNL. Hence, the selected molecules, especially **20**, could be developed and further evaluated as potential drug candidates for treating onchocerciasis. More so, FBZ remains promising and could still be improved to address the problem of oral bioavailability and the threats posed by its toxicity level.

ACKNOWLEDGMENT

All authors are well acknowledged for their contributions. No funding was received for this study.

AUTHORS' CONTRIBUTION

All authors conceived and designed the study. **Fabian Audu Ugbe** carried out the study and drafted the manuscript. **Gideon Adamu Shallangwa** conducted the technical editing. All authors read and approved the final manuscript.

DATA AVAILABILITY

All data related to this study are included herein.

CONFLICT OF INTEREST

The authors declare no conflict of interest.

REFERENCES

1. Ngwewondo A, Scandale I, Specht S. Onchocerciasis drug development: from preclinical models to humans. *Parasitol Res.* 2021;120(12):3939-64. doi:10.1007/s00436-021-07307-4
2. Ugbe FA, Shallangwa GA, Uzairu A, Abdulkadir I. Theoretical modeling and design of some pyrazolopyrimidine derivatives as *Wolbachia* inhibitors, targeting lymphatic filariasis and onchocerciasis. *In Silico Pharmacol.* 2022;10(1):8. doi:10.1007/s40203-022-00123-3
3. Metuge JA, Nyongbela KD, Mbah JA. Anti-Onchocerca activity and phytochemical analysis of an essential oil from *Cyperus articulatus* L. *BMC Complement Altern Med.* 2014;14:223. doi:10.1186/1472-6882-14-223
4. Samje M, Metuge J, Mbah J, B. Nguesson, Cho-Ngwa F. In vitro anti-Onchocerca ochengi activities of extracts and chromatographic fractions of *Craterispermum laurinum* and *Morinda lucida*. *BMC Complement Altern Med.* 2014;14:325. doi:10.1186/1472-6882-14-325
5. Metuge JA, Babiaka SB, Mbah JA, Ntie-Kang F, Ayimele GA, Cho-Ngwa F. Anti-onchocerca Metabolites from *Cyperus articulatus*: Isolation, In Vitro Activity and In Silico 'Drug-Likeness'. *Nat Prod Bioprospect.* 2014;4(4):243-9. doi:10.1007/s13659-014-0023-5
6. McGillan P, Berry NG, Nixon L, Leung SC, Webborn PJH, Wenlock MC, et al. Development of Pyrazolopyrimidine Anti-*Wolbachia* Agents for the Treatment of Filariasis. *ACS Med Chem Lett.* 2021;12(9):1421-6. doi:10.1021/acsmchemlett.1c00216
7. Sungpradit S, Sanprasert V. Lymphatic filariasis. In Misra G, Srivastava V, editors. *Molecular Advancements in Tropical Diseases Drug Discovery.* Amsterdam: Elsevier; 2020. p. 65-94. doi:10.1016/B978-0-12-821202-8.00004-9
8. Sainas S, Dosio F, Boschi D, Lolli ML. Targeting Human Onchocerciasis: Recent Advances Beyond Ivermectin. *Annu Rep Med Chem.* 2018;51:1-38. doi:10.1016/bs.armc.2018.08.001
9. Akama T, Freund YT, Berry P, Carter DE, Easom E, Jarnagin K, et al. Macrofilaricidal Benzimidazole-Benzoxaborole Hybrids as an Approach to the Treatment of River Blindness: Part 1. Amide Linked Analogs *ACS Infect Dis.* 2020;6(2):173-9. doi:10.1021/acsinfectdis.9b00396
10. Carter DS, Jacobs RT, Freund Y, Berry P, Akama T, Easom EE, et al. Macrofilaricidal Benzimidazole-Benzoxaborole Hybrids as an Approach to the Treatment of River Blindness: Part 2. Ketone Linked Analogs. *ACS Infect Dis.* 2020;6(2):180-5. doi:10.1021/acsinfectdis.9b00397
11. Adeniji SE, Arthur DE, Abdullahi M, Abdullahi A, Ugbe FA. Computer-aided modeling of triazole analogues, docking studies of the compounds on DNA gyrase enzyme and design of new hypothetical compounds with efficient activities. *J Biomol Struct Dyn.* 2020;40(9):4004-20. doi:10.1080/07391102.2020.1852963
12. Ibrahim MT, Uzairu A, Shallangwa GA, Uba S. Lead Identification of Some Anti-Cancer Agents with Prominent Activity Against Non-small Cell Lung Cancer (NSCLC) and Structure-Based Design. *Chem Afr.* 2020;3:1023-44. doi:10.1007/s42250-020-00191-y
13. Ugbe FA, Shallangwa GA, Uzairu A, Abdulkadir I. Activity modeling, molecular docking and pharmacokinetic studies of some boron-pleuromutilins as anti-wolbachia agents with potential for treatment of filarial diseases. *Chem Data Collect.* 2021;36:100783. doi:10.1016/j.cdc.2021.100783
14. Ibrahim MT, Uzairu A, Uba S, Shallangwa GA. Design of more potent quinazoline derivatives as EGFRWT inhibitors for the treatment of NSCLC: a computational approach. *Future J Pharm Sci.* 2021;7:140. doi:10.1186/s43094-021-00279-3
15. Lipinski CA, Lombardo F, Dominy BW, Feeney PJ. Experimental and computational approaches to estimate solubility and permeability in drug discovery and development settings. *Adv Drug Deliv Rev.* 2001;46(1-3):3-26. doi:10.1016/s0169-409x(00)00129-0

16. Edache EI, Uzairu A, Mamza PA, Shallangwa GA. Computational modeling and analysis of the Theoretical structure of Thiazolino 2-pyridone amide inhibitors for *Yersinia pseudotuberculosis* and *Chlamydia trachomatis* Infectivity. *Bull Sci Res.* 2022;4(1):14-39. doi:[10.54392/bsr2212](https://doi.org/10.54392/bsr2212)
17. Perbandt M, Höppner J, Burmeister C, Lüersen K, Betzel C, Liebau E. Structure of the extracellular glutathione S-transferase OvGST1 from the human pathogenic parasite *Onchocerca volvulus*. *J Mol Biol.* 2008;377(2):501-11. doi:[10.1016/j.jmb.2008.01.029](https://doi.org/10.1016/j.jmb.2008.01.029)
18. Perbandt M, Höppner J, Betzel C, Walter RD, Liebau E. Structure of the major cytosolic glutathione S-transferase from the parasitic nematode *Onchocerca volvulus*. *J Biol Chem.* 2005;280(13):12630-6. doi:[10.1074/jbc.m413551200](https://doi.org/10.1074/jbc.m413551200)
19. Baell JB, Holloway GA. New substructure filters for removal of pan assay interference compounds (PAINS) from screening libraries and for their exclusion in bioassays. *J Med Chem.* 2010;53(7):2719-40. doi:[10.1021/jm901137j](https://doi.org/10.1021/jm901137j)
20. Pires DE, Blundell TL, Ascher DB. pkCSM: Predicting Small-Molecule Pharmacokinetic and Toxicity Properties Using Graph-Based Signatures. *J Med Chem.* 2015;58(9):4066-72. doi:[10.1021/acs.jmedchem.5b00104](https://doi.org/10.1021/acs.jmedchem.5b00104)
21. Yang H, Lou C, Sun L, Li J, Cai Y, Wang, Z, et al. admetSAR 2.0: web-service for prediction and optimization of chemical ADMET properties. *Bioinformatics.* 2019;35(6):1067-9. doi:[10.1093/bioinformatics/bty707](https://doi.org/10.1093/bioinformatics/bty707)
22. Daina A, Michielin O, Zoete V. SwissADME: a free web tool to evaluate pharmacokinetics, drug-likeness and medicinal chemistry friendliness of small molecules. *Sci Rep.* 2017;7(1):42717. doi:[10.1038/srep42717](https://doi.org/10.1038/srep42717)
23. Lee J, Cheng X, Swails JM, Yeom MS, Eastman PK, Lemkul JA, et al. CH CHARMM-GUI Input Generator for NAMD, GROMACS, AMBER, OpenMM, and CHARMM/OpenMM Simulations Using the CHARMM36 Additive Force Field. *J Chem Theory Comput.* 2016;12(1):405-13. doi:[10.1021/acs.jctc.5b00935](https://doi.org/10.1021/acs.jctc.5b00935)
24. Wang X, Dong H, Qin Q. QSAR models on aminopyrazole-substituted resorcyate compounds as Hsp90 inhibitors. *J Comput Sci Eng.* 2020;48:1146-56.
25. Ugbe FA, Shallangwa GA, Uzairu A, Abdulkadir I. Theoretical activity prediction, structure-based design, molecular docking and pharmacokinetic studies of some maleimides against *Leishmania donovani* for the treatment of leishmaniasis. *Bull Natl Res Cent.* 2020;46:92. doi:[10.1186/s42269-022-00779-z](https://doi.org/10.1186/s42269-022-00779-z)
26. Abdullahi SA, Uzairu A, Shallangwa GA, Uba S, Umar AB. In-silico activity prediction, structure-based drug design, molecular docking and pharmacokinetic studies of selected quinazoline derivatives for their antiproliferative activity against triple negative breast cancer (MDA-MB231) cell line. *Bull Natl Res Cent.* 2022;46:2. doi:[10.1186/s42269-021-00690-z](https://doi.org/10.1186/s42269-021-00690-z)
27. Sun Y, Yang AW, Hung A, Lenon GB. Screening for a Potential Therapeutic Agent from the Herbal Formula in the 4th Edition of the Chinese National Guidelines for the Initial-Stage Management of COVID-19 via Molecular Docking. *Evid Based Complement Alternat Med.* 2020;3219840. doi:[10.1155/2020/3219840](https://doi.org/10.1155/2020/3219840)
28. Abraham MJ, Gready JE. Optimization of parameters for molecular dynamics simulation using smooth particle-mesh Ewald in GROMACS 4.5. *J Comput Chem.* 2011;32(9):2031-40. doi:[10.1002/jcc.21773](https://doi.org/10.1002/jcc.21773)
29. Bai Q, Tan S, Xu T, Liu H, Huang J, Yao X. MolAICal: a soft tool for 3D drug design of protein targets by artificial intelligence and classical algorithm. *Brief Bioinformatics.* 2020;22(3):bbaa161. doi:[10.1093/bib/bbaa161](https://doi.org/10.1093/bib/bbaa161)
30. Edache EI, Uzairu A, Mamza PA, Shallangwa GA. A Comparative QSAR Analysis, 3D-QSAR, Molecular Docking And Molecular Design Of Iminoguanidine-Based Inhibitors Of HemO: A Rational Approach To Antibacterial Drug Design. *J Drugs Pharm Sci.* 2020;4(3):21-36. doi:[10.31248/JDPS2020.036](https://doi.org/10.31248/JDPS2020.036)
31. Ugbe FA, Shallangwa GA, Uzairu A, Abdulkadir I. A 2-D QSAR Modeling, Molecular Docking Study and Design of 2-Arylbenzimidazole Derivatives as Novel *Leishmania* Inhibitors: A Molecular Dynamics Study. *Adv J Chem Sect A.* 2023;6(1):50-64. doi:[10.22034/ajca.2023.365873.1337](https://doi.org/10.22034/ajca.2023.365873.1337)